Redox Biology 51 (2022) 102253

Contents lists available at ScienceDirect

Redox Biology

journal homepage: www.elsevier.com/locate/redox

ASIC1a senses lactate uptake to regulate metabolism in neurons

Ivana Savic Azoulay [a,b,1], Xin Qi [a,1], Maya Rozenfeld [b], Fan Liu [a], Qin Hu [a], Tsipi Ben Kasus Nissim [b], Alexandra Stavsky [b], Michael X. Zhu [c,***], Tian-Le Xu [a,d,e,f,**], Israel Sekler [b,*]

[a] Department of Anatomy and Physiology, Shanghai Jiao Tong University School of Medicine, Shanghai, 200025, China
[b] Department of Physiology and Cell Biology, Faculty of Health Sciences, Ben-Gurion University of the Negev, Beer-Sheva, 84105, Israel
[c] Department of Integrative Biology and Pharmacology, McGovern Medical School, The University of Texas Health Science Center at Houston, Houston, 77030, USA
[d] Center for Brain Science of Shanghai Children's Medical Center, Shanghai Jiao Tong University School of Medicine, Shanghai, 200127, China
[e] Shanghai Research Center for Brain Science and Brain Inspired Intelligence, Shanghai, 201210, China
[f] Co-Innovation Center of Neuroregeneration, Nantong University, Nantong, Jiangsu 226001, China

ARTICLE INFO

Keywords:
ASIC1a
Cytosolic Na^+ signaling
Cytosolic Ca^{2+} signaling
Mitochondrial Na^+ signaling
Mitochondrial Ca^{2+} signaling
NCLX
Lactate
Acidification

ABSTRACT

Lactate is a major metabolite largely produced by astrocytes that nourishes neurons. ASIC1a, a Na^+ and Ca^{2+}-permeable channel with an extracellular proton sensing domain, is thought to be activated by lactate through chelation of divalent cations, including Ca^{2+}, Mg^{2+} and Zn^{2+}, that block the channel pore. Here, by monitoring lactate-evoked H^+ and Ca^{2+} transport in cultured mouse cortical and hippocampal neurons, we find that stereo-selective neuronal uptake of L-lactate results in rapid intracellular acidification that triggers H^+ extrusion to activate plasma membrane ASIC1a channels, leading to propagating Ca^{2+} waves into the cytosol and mitochondria. We show that lactate activates ASIC1a at its physiological concentrations, far below that needed to chelate divalent cations. The L-isomer of lactate exerts a much greater effect on ASIC1a-mediated activity than the D-isomer and this stereo-selectivity arises from lactate transporters, which prefer the physiologically common L-lactate. The lactate uptake in turn results in intracellular acidification, which is then followed by a robust acid extrusion. The latter response sufficiently lowers the pH in the vicinity of the extracellular domain of ASIC1a to trigger its activation, resulting in cytosolic and mitochondrial Ca^{2+} signals that accelerate mitochondrial respiration. Furthermore, blocking ASIC1a led to a robust mitochondrial ROS production induced by L-lactate. Together our results indicate that ASIC1a is a metabolic sensor, which by sensing extracellular pH drop triggered by neuronal lactate uptake with subsequent proton extrusion, transmits a Ca^{2+} response that is propagated to mitochondria to enhance lactate catabolism and suppress ROS production.

1. Introduction

Acid sensing ion channels (ASICs) are proton-gated sodium-selective channels mainly found in the central and peripheral nervous systems [1,2] but with some expression also in other tissue types [3,4]. So far, 6 subtypes of ASICs have been described, with ASIC1a being the major subtype expressed in neurons of the central nervous system [5]. In addition to conducting Na^+, ASIC1a also exhibits Ca^{2+} permeability [5–7]. Protons, even by a small concentration change within the physiological range of 7.4–7.0 [8], can act at the extracellular domain of ASIC1a to cause channel pore opening, triggering Na^+ and Ca^{2+} influx into the cell [1]. ASIC1a activity is inhibited by divalent cations, such as Zn^{2+} and Ca^{2+} (at high concentrations) [5,9,10], but enhanced or potentiated by metabolites, e.g., spermine [11,12] and lactate [13–15]. Lactate is thought to be primarily produced by astrocytes and then delivered to neurons [16]. The lactate effect on ASICs was believed to be primarily associated with its ability to chelate divalent cations in the extracellular solution and thereby reducing the divalent cation block of the ASIC1a activity [13]. Lactate is a weak chelator and therefore the concentration required for ASIC1a activation were supra physiological,

* Corresponding author.
** Corresponding author. Department of Anatomy and Physiology, Shanghai Jiao Tong University School of Medicine, Shanghai, 200025, China.
*** Corresponding author.
E-mail addresses: Michael.X.Zhu@uth.tmc.edu (M.X. Zhu), xu-happiness@shsmu.edu.cn (T.-L. Xu), sekler@bgu.ac.il (I. Sekler).
[1] These authors contributed equally to this work.

https://doi.org/10.1016/j.redox.2022.102253
Received 31 August 2021; Received in revised form 25 January 2022; Accepted 26 January 2022
Available online 29 January 2022

well above the physiological milieu of lactate in the brain. As would be predicted by the chelation effect, both enantiomers of lactate, the D- and the biologically common L-isomers, activated ASIC1a when applied at a high concentration (15 mM) [13]. However, in the physiological conditions lactate concentration in the brain reaches a much lower concentration of ~2–5 mM, implicating that neither L- nor D-isomer of lactate is likely to modulate ASIC1a through affecting divalent cation binding in the normal brain. Thus, whether and how the two enantiomers of lactate regulate ASIC1a during normal brain metabolic activities remain elusive.

Lactate is taken up by neurons primarily by the lactate transporter [16] and being a weak acid, it can acidify the neuronal cytosol. However, to what extent this effect influences ASIC1a activity is poorly understood. Inside the cell, lactate is converted to pyruvate in the processes of mitochondrial oxidative phosphorylation. Calcium is a critical regulator of oxidative phosphorylation as a rise in mitochondrial Ca^{2+} - $[Ca^{2+}]_m$ stimulates at least 3 enzymes of the Krebs cycle [17], linking Ca^{2+} signaling to ATP production [18]. Thus, the extracellular presence of physiologically relevant low concentrations of lactate could affect Ca^{2+} signaling, redox and metabolic activity in a number of ways, by modulating ASIC1a and consequent cytosolic - $[Ca^{2+}]_c$ and $[Ca^{2+}]_m$ levels [8] and/or providing the carbon source to fuel ATP production. Here we asked if extracellular lactate at its low physiological concentrations and the normal neutral pH (pH 7.4) can evoke $[Ca^{2+}]_m$ signals and thereby control their metabolic activity and whether these signals are linked to ASIC1a activity. In this context, we also asked if the physiologically relevant intracellular lactate uptake or metabolism can evoke local extracellular acidification leading to ASIC1a activation necessary for a plasma membrane - mitochondria crosstalk that underpins lactate regulation of neuronal metabolic activity.

We find that in primary hippocampal and cortical neurons, physiological L-lactate (2 and 5 mM at pH 7.4) but not D-lactate, triggers ASIC1a dependent $[Ca^{2+}]_c$ transients that are propagated to the mitochondria. ASIC1a inhibition by ASIC1a specific inhibitor - Psalmotoxin (PcTX1) or *Asic1a* gene knockout (KO) blocks these Ca^{2+} signals. We show that ASIC1a dependent $[Ca^{2+}]_c$ and $[Ca^{2+}]_m$ signals are evoked when L-lactate is transported into the neuron. Moreover, we demonstrate that the pH 7.4 L-lactate solution subsequently triggers intracellular acidification, which is followed by near membrane acidification at the extracellular side. Finally, we show that the L-lactate-dependent activation of ASIC1a is capable of enhancing mitochondrial respiration and suppressing ROS elevation.

2. Results

We first asked if a racemic mixture of D- and L-lactate at the physiological concentration (5 mM) would activate ASIC1a-dependent $[Ca^{2+}]_c$ increase (Fig. 1A). Cultured primary mouse hippocampal neurons, loaded with the Ca^{2+} specific dye Fura-2, were first super-fused with the Ringer's solution and then switched to a Ringer's solution in which glucose was replaced with 5 mM racemic (DL) lactic acid. The application of the racemic DL-lactate mixture at pH 7.4 induced robust $[Ca^{2+}]_c$ transients, which were suppressed by treating the neurons with the ASIC1a blocker PcTX1 (Fig. 1B, C). As with the $[Ca^{2+}]_c$ measurement, we also monitored $[Ca^{2+}]_m$ signals in response to racemic lactate in neurons loaded with the mitochondrion-targeted Ca^{2+} dye Rhod-2.

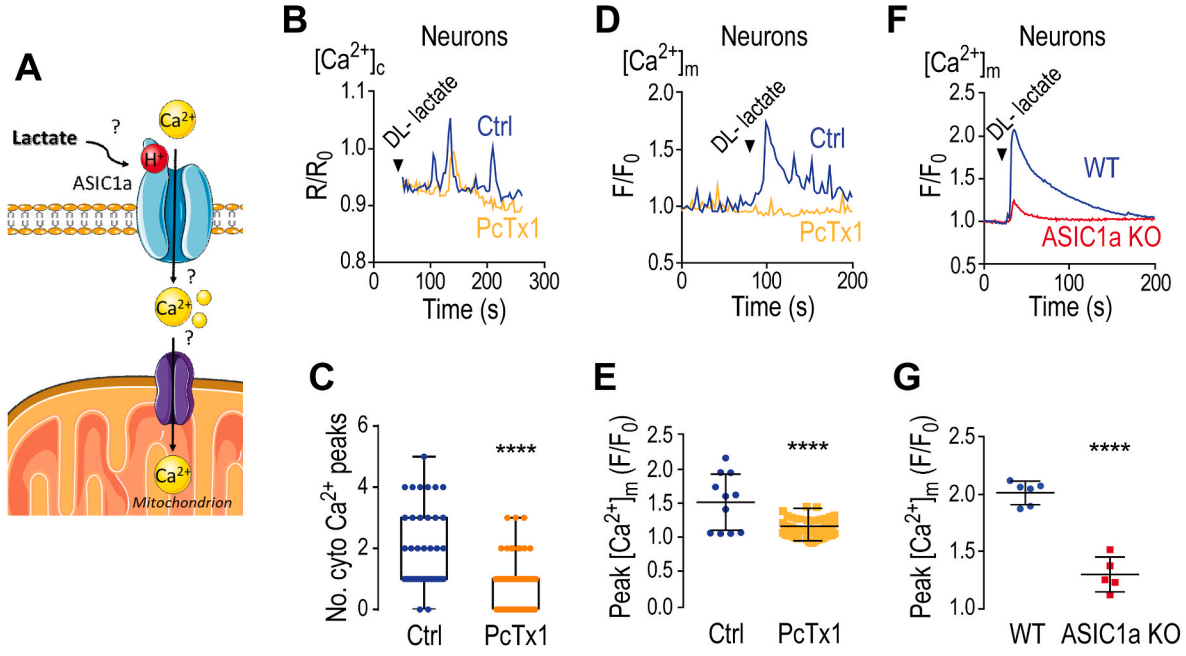

Fig. 1. Racemic lactate triggers ASIC1a dependent $[Ca^{2+}]_c$ and $[Ca^{2+}]_m$ signals.
(A) Illustration of the figure hypothesis;
(B) Representative Fura-2 ratio traces for $[Ca^{2+}]_c$ changes monitored in WT primary cultured hippocampal neurons (DIV 10–15) without and with pretreatment of the selective ASIC1a inhibitor PcTx1 (20 nM, 120 s). Neurons were loaded with Fura-2AM (1 μM) and initially superfused with Ringer's solution at pH 7.4. Then, the superfusion was switched to Ringer's solution of pH 7.4 with an addition of DL-lactate (5 mM) as indicated by the arrowhead;
(C) Quantification of the number of cytosolic (cyto) Ca^{2+} peaks (transients) per 180-s time period measured as in (B) for WT neurons untreated (n = 39) and treated (n = 77); Box and whiskers plot show maximal and minimal values and all data points;
(D) Representative Rhod-2 fluorescence traces for $[Ca^{2+}]_m$ changes in Rhod-2 AM (1 μM)-loaded WT neurons untreated and treated with PcTX1. Superfusion was switched to pH 7.4 Ringer's solution with DL-lactate;
(E) Quantification of peak $[Ca^{2+}]_m$ based on F/F_0 during the maximum phases as in (D) for WT neurons untreated (n = 11) and treated with PcTX1 (n = 65);
(F) Representative Rhod-2 fluorescence traces for $[Ca^{2+}]_m$ changes in response to direct puffing of the pH 7.4-DL- lactate solution in primary cultured WT and KO cortical neurons;
(G) Quantification of peak $[Ca^{2+}]_m$ based on F/F_0 during the maximum phases as in (F) for WT (n = 6) and KO cortical neurons (n = 5);
All summary data represent mean ± SD, ****$p < 0.0001$.

We detected robust $[Ca^{2+}]_m$ transients evoked by DL-lactate, which were again diminished by the treatment with PcTX1 (Fig. 1D, E). Similarly, the DL-lactate-induced $[Ca^{2+}]_m$ response seen in wild type (WT) cortical neurons was largely missing in *Asic1a* KO neurons (Fig. 1F, G). These data indicate that the physiological concentration of racemic lactate invokes ASIC1a-dependent Ca^{2+} signals in both the cytosol and mitochondria of hippocampal and cortical neurons, despite the maintenance of the extracellular solution pH at 7.4.

Lactate is thought to enhance ASIC1a activation by acting as a chelator of divalent cations in the extracellular space and thereby reducing the free concentration of divalent cations that inhibit ASIC1a channel function [5,9,10]. If this were true, then the L- and D- enantiomers of lactate would have similar effects on ASIC1a and the consequent Ca^{2+} signals. To test this hypothesis, we performed similar experiments as in Fig. 1, but with the use of either D- or L-lactate (Fig. 2A–D). To our surprise, whereas the D-isomer failed to evoke Ca^{2+} signals in both the cytosol and mitochondria, L-lactate in its pure form induced similarly strong $[Ca^{2+}]_c$ and $[Ca^{2+}]_m$ transients like the racemic mixture of DL-lactate (Fig. 2A–D). Again, the L-lactate-evoked $[Ca^{2+}]_m$ transients were diminished by the treatment with PcTX1 (Fig. 2 E, F) and dramatically lost in neurons from *Asic1a* KO mice (Fig. 2G, H). Therefore, the ASIC1a-dependent $[Ca^{2+}]_c$ and $[Ca^{2+}]_m$ signals activated by lactate show stereo selectivity and are only evoked by the physiologically more common L-isomer. This selectivity in stereochemistry of the compound argues against divalent cation chelation as the major mechanism of lactate activation of ASIC1a and the consequent cytosolic and mitochondrial Ca^{2+} signaling.

The stereo-selectivity of lactate on ASIC1a activation may result from a direct stereo specific ligand binding to the channel or an indirect mechanism. Since the direct lactate interaction with ASIC1a channels had been previously ruled out [13], we focused on indirect mechanisms. It is known that lactate is taken up by neurons through the action of lactate transporters that exhibit greater selectivity for L-than D-lactic acid [19]. Being a weak acid, the cellular uptake of lactate also triggers a cytosolic pH (pH_c) drop [19]. Therefore, we hypothesized that the stereo-selective activation of ASIC1a by the L-isomer of lactate could occur as a consequence of stereo-selective uptake of L-lactate by the lactate transporter and the subsequent decrease in pH_c (Fig. 3A). To test this hypothesis, we first examined the effects of L- and D-lactate on pH_c of cultured mouse hippocampal neurons loaded with the cytosolic pH sensitive dye BCECF. With the Ringer's solution switched to the one containing either L- or D-lactate (5 mM) at pH 7.4 by super-fusion, pH_c decreased in a time-dependent fashion; however, the decrease was faster and more pronounced in response to L-lactate than D-lactate (Fig. 3B, C). To check if lactate transport is necessary for the lactate-induced cytosolic acidification, we used the lactate transporter inhibitor α-Cyano-4-hydroxycinnamate (CIN4). In the presence of CIN4 (250 nM), pH_c drop was strongly attenuated no matter if it was induced by the racemic DL-lactate mixture (Fig. 3D, E) or just the L-lactate isomer (Fig. 3F, G). These results confirm the stereo-selective uptake of L-lactate by lactate transporters in mouse hippocampal neurons, which causes a decrease in pH_c.

Next, we asked if L-lactate uptake through lactate transporters underlies the lactate-induced ASIC1a-dependent Ca^{2+} signals. We compared the $[Ca^{2+}]_c$ and $[Ca^{2+}]_m$ responses to L-lactate in the presence and absence of CIN4. As expected, inhibiting lactate transport with CIN4

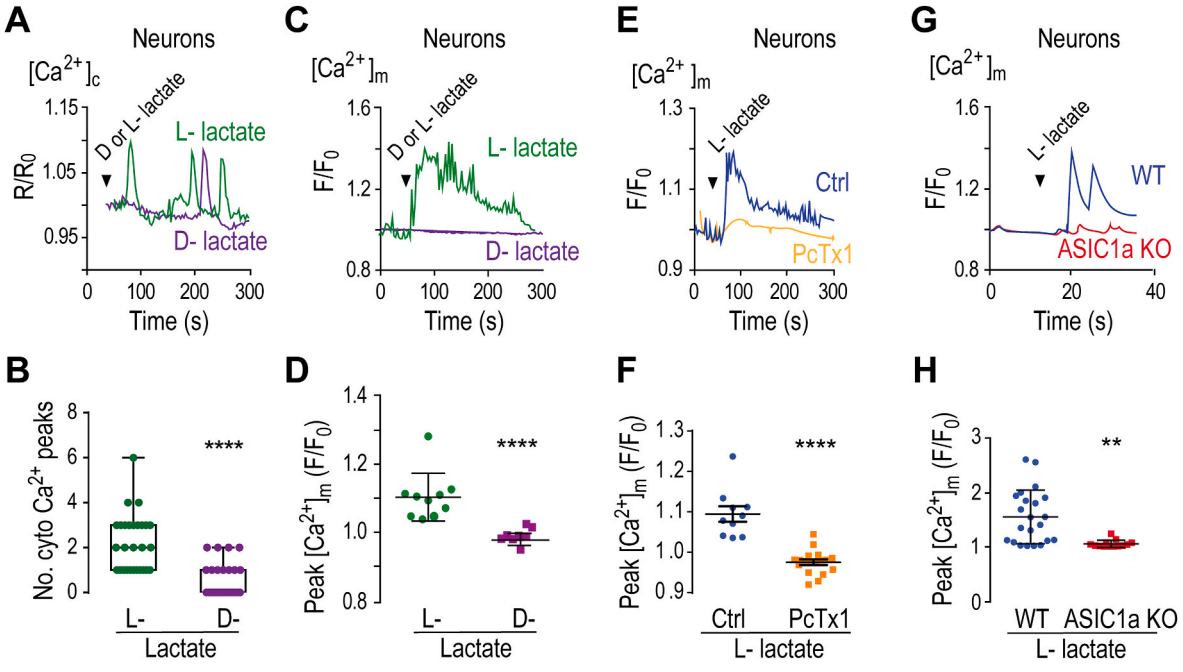

Fig. 2. L-lactate triggers ASIC1a dependent cytosolic and mitochondrial Ca^{2+} signals.

(A) Representative Fura-2 ratio traces for $[Ca^{2+}]_c$ changes monitored in WT primary cultured hippocampal neurons as in Fig. 1. Neurons were loaded with Fura-2 AM (1 μM) and initially superfused with Ringer's solution at pH 7.4. Then, the superfusion was switched to Ringer's solution of pH 7.4 with an addition of either D- or L-lactate (5 mM) as indicated by the arrowhead;

(B) Quantification of the number of cytosolic (cyto) Ca^{2+} peaks (transients) as shown in (A), calculated and presented as in Fig. 1C, for WT neurons stimulated with L- (n = 28) and D-lactate (n = 26);

(C) Representative Rhod-2 fluorescence traces for $[Ca^{2+}]_m$ changes in WT neurons in response to superfusion of pH 7.4 Ringer's solution with D- or L-lactate;

(D) Quantification of peak $[Ca^{2+}]_m$ based on F/F_0 during the maximum phases as in (C) for WT neurons treated with L- (n = 10) and D-lactate (n = 9);

(E) Representative Rhod-2 fluorescence traces for $[Ca^{2+}]_m$ changes in response to L-lactate Ringer's solution on WT neurons untreated and treated;

(F) Quantification of peak $[Ca^{2+}]_m$ based on F/F_0 during the maximum phases as in (E) for WT neurons untreated (n = 10) and treated (n = 12);

(G) Representative Rhod-2 fluorescence traces for $[Ca^{2+}]_m$ changes in response to direct puffing of the pH 7.4-L- lactate solution to WT and KO cortical neurons;

H) Quantification of $[Ca^{2+}]_m$ based on F/F_0 during the maximum phases as in (G) for WT (n = 22) and KO neurons (n = 11);

All summary data represent mean ± SD, $^{**}p < 0.01$ $^{****}p < 0.0001$.

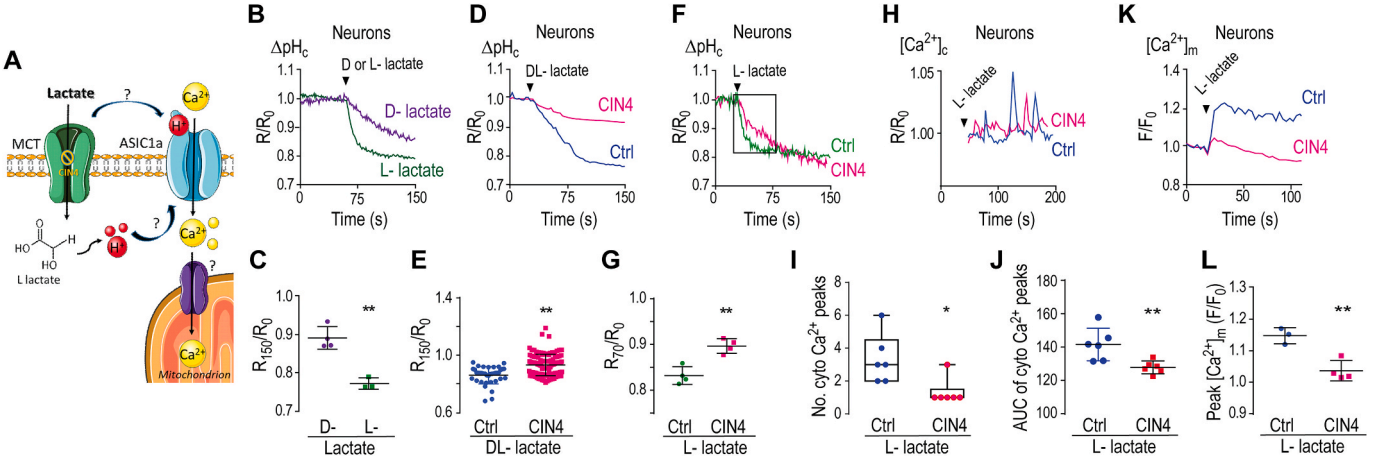

Fig. 3. Lactate uptake is crucial for ASIC1a dependent $[Ca^{2+}]_c$ and $[Ca^{2+}]_m$ elevation in neurons.
(A) Illustration of the figure hypothesis;
(B) Representative BCECF fluorescence traces for cytosolic pH changes (ΔpH_c) monitored in WT primary cultured hippocampal neurons. Neurons were loaded with BCECF-AM (25 μM). D- or L-lactate (5 mM) in Ringer's solution of pH 7.4 was applied by superfusion as indicated by the arrowhead;
(C) Quantification of BCECF fluorescence ratio at 90 s after the addition of lactate as measured in (B) for WT neurons treated with D- (n = 4) or L-lactate (n = 3);
(D) Representative BCECF fluorescence traces for ΔpH_c in WT neurons untreated (*blue*) or pretreated with CIN4 (250 nM, 1 h incubation, *red*) in response to racemic DL-lactate (5 mM) in Ringer's solution of pH 7.4;
(E) Quantification of BCECF fluorescence ratio at 90 s after the addition of DL-lactate for conditions shown in (D) of WT neurons untreated (n = 32) and treated with CIN4 (n = 56);
(F) Representative BCECF fluorescence traces for ΔpH_c in WT neurons untreated (*green*) or pretreated with CIN4 (250 nM, *red*) in response to L-lactate in Ringer's solution of pH 7.4;
(G) Quantification of BCECF fluorescence ratio at 40 s after the addition of L-lactate for conditions shown in (F) of WT neurons untreated (n = 4) and treated with CIN4 (n = 4). (H) Representative Fura-2 ratio traces for $[Ca^{2+}]_c$ monitored in WT primary cultured hippocampal neurons as in Fig. 1. Fura-2-loaded neurons were untreated (*blue*) or pretreated with CIN4 (250 nM, *red*). L-lactate (5 mM) in Ringer's solution of pH 7.4 was applied as indicated; (I) Quantification of the number of cytosolic (cyto) Ca^{2+} peaks (transients) measured as in (H), calculated and presented as in Fig. 1C, for WT neurons untreated (n = 6) and treated with CIN4 (n = 6);
(J) Quantification of $[Ca^{2+}]_c$ signals, presented as area under the curve (AUC) of the $[Ca^{2+}]_c$ transients over 120 s measured as in (H) for WT neurons untreated (n = 6) and treated with CIN4 (n = 6); (K) Representative Rhod-2 fluorescence traces for $[Ca^{2+}]_m$ changes in WT neurons untreated (*blue*) or treated with CIN4 (250 nM, *red*) in response to superfusion of L-lactate (5 mM) in Ringer's solution of pH 7.4; (L) Quantification of peak $[Ca^{2+}]_m$ based on F/F_0 during the maximum phases as in (K) for WT neurons untreated (n = 3) and treated with CIN4 (n = 4); All summary data represent mean ± SD. *p < 0.05, **p < 0.01.

diminished not only the L-lactate-evoked Ca^{2+} transients in the cytosol (Fig. 3H–J), but also that in the mitochondria (Fig. 3K, L). These results provide strong support to the idea that at physiological extracellular pH, lactate activates ASIC1a channels through an indirect mechanism involving initially L-lactate uptake by the lactate transporter, which then leads to ASIC1a activation that triggers a $[Ca^{2+}]_c$ increase followed by a $[Ca^{2+}]_m$ response.

L-lactate uptake is mainly carried out by monocarboxylate transporters (MCTs). Among the four mammalian MCTs, MCT2 (or SLC16A7) has the highest affinity to L-lactate (Km ~0.7 mM) and is highly expressed in the brain [20,21]. To ascertain that the lactate dependent Ca^{2+} rise is linked to MCT2, we knocked down the expression of this transporter in cortical neurons using MCT2 specific shRNA (shMCT2) (Supplementary Fig. 1A, B) and found that the decrease in MCT2 expression diminished the lactate dependent $[Ca^{2+}]_c$ and $[Ca^{2+}]_m$ responses (Supplementary Fig. 1C-F). These findings indicate that MCT2 is linked to lactate transport that underlies the ASIC1a-dependent $[Ca^{2+}]_c$ and $[Ca^{2+}]_m$ elevations. We also asked if the administration of L-lactate at the lower physiological range of 2 mM is capable of eliciting the pH_c decrease and ASIC1a $[Ca^{2+}]_m$ response and found it to be the case, albeit the responses being less robust than that elicited by 5 mM L-lactate (Supplementary Fig. 2A-F).

However, a pH_c drop does not necessarily lead to ASIC1a activation because the proton sensing sites are all located in the extracellular loop of ASIC1a. We reasoned that the pH_c drop generated by dissociation of H^+ from lactate and by metabolic processing of lactate may be followed by H^+ extrusion and once outside, the protons would trigger ASIC1a activation. Given that the global extracellular pH is buffered by HEPES in the Ringer's solution, as well as endogenous pH buffers in cerebrospinal or interstitial fluid, the local pH changes in the vicinity of ASIC1a extracellular loop would be more relevant to lactate-induced ASIC1a activation. To monitor if extracellular acidification occurs in the vicinity of ASIC1a in response to lactate, we used a cDNA construct that encodes ASIC1a with pHluorin inserted in between residues 298 and 299 in the extracellular loop (pHluorin-ASIC1a) [22]. Upon protonation, pHluorin exhibits a decrease in fluorescence intensity, as shown by the rapid and large decrease in pHluorin-ASIC1a expressing CHO cells upon switching the extracellular pH from 7.4 to 6.0 (Fig. 4A). Interestingly, the application of 5 mM L-lactate at pH 7.4 in the Ringer's solution also caused a clearly detectable decrease in the F/F_0, albeit to a much lesser extent than that caused by the pH 6.0 solution (Fig. 4A). A similar decrease was also detected in CHO cells that expressed extracellularly pHluorin-tagged GluR2 (an AMPA receptor subunit) (Fig. 4B), suggesting that the L-lactate elicited near membrane extracellular acidification is a general effect, rather than a phenomenon specifically dependent on the expression or function of ASIC1a.

We then compared extracellular acidification induced by 5 mM of L-lactate versus that of D-lactate and found that the L-isomer induced not only a faster acidification but also a greater maximal change than the D-isomer (Fig. 4C–E). To determine the potential source of the near

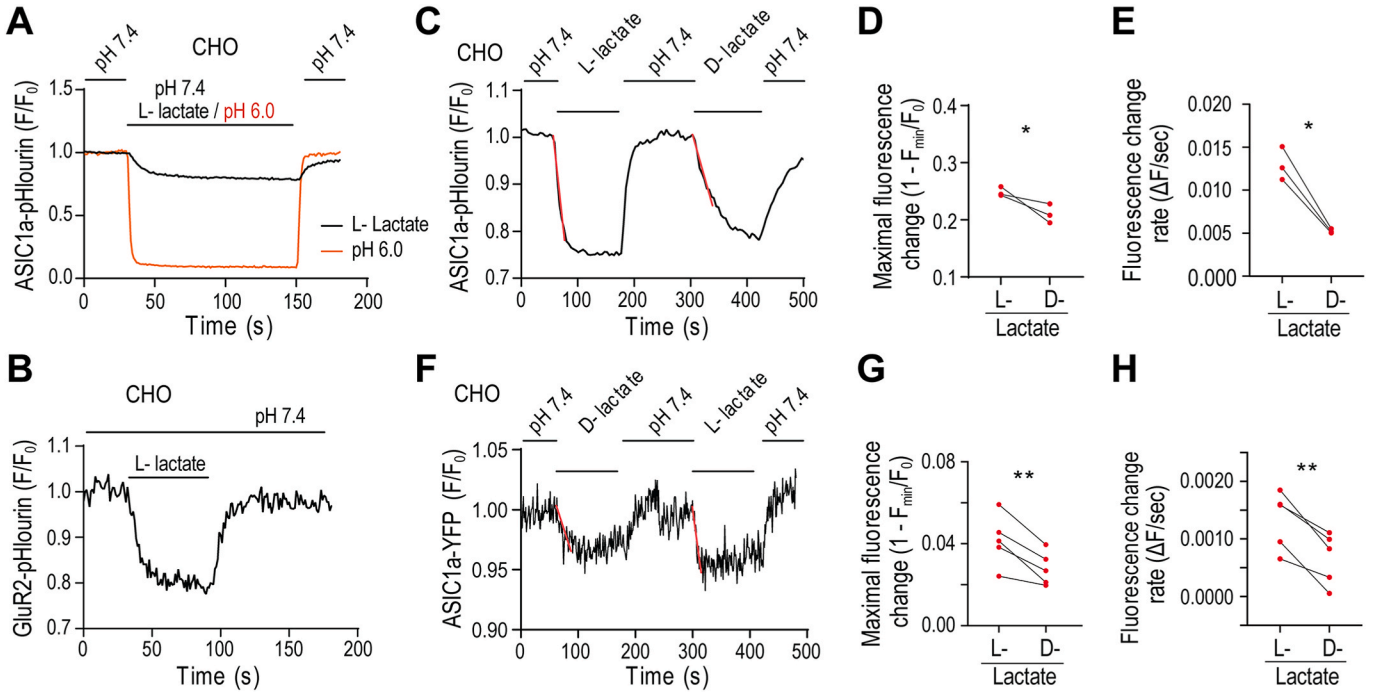

Fig. 4. L-lactate evoked intracellular acidification is followed by extracellular acidification.

(A) Representative pHlourin fluorescence traces for near membrane extracellular pH changes monitored in CHO cells transfected with the ASIC1a-pHlourin plasmid. The cells were superfused with a Ringer's solution of pH 6.0 or L-lactate (5 mM) in Ringer's solution of pH 7.4 (wash) as indicated by the horizontal bars;

(B) Representative pHlourin fluorescence traces for near membrane extracellular pH changes monitored in CHO cells transfected with the GluR2-pHlourin plasmid. The cells were superfused with L-lactate (5 mM) in Ringer's solution of pH 7.4 as indicated;

(C) Representative pHlourin fluorescence traces for near membrane extracellular pH changes monitored in CHO cells transfected with the ASIC1a-pHlourin plasmid. The cells were superfused with L- or D-lactate (5 mM) in Ringer's solution of pH 7.4 as indicated;

(D) Quantification of maximal pHlourin fluorescence change ($1\text{-}F_{min}/F_0$) for extracellular acidification triggered by L- (n = 3) or D-lactate (n = 3) in Ringer's solution of pH 7.4;

(E) Quantification of the rate of pHlourin fluorescence change (ΔF/sec) for extracellular acidification triggered by L- (n = 3) or D-lactate (n = 3) in Ringer's solution of pH 7.4;

(F) Representative YFP fluorescence traces for near membrane cytosolic pH changes monitored in CHO cells transfected with the ASIC1a-YFP plasmid. The cells were superfused with L- or D-lactate (5 mM) in Ringer's solution of pH 7.4 as indicated;

(G) Quantification of maximal YFP fluorescence change ($1\text{-}F_{min}/F_0$) for near membrane ΔpH_c triggered by L- (n = 5) or D-lactate (n = 5) in Ringer's solution of pH 7.4;

(H) Quantification of the rate of YFP fluorescence change (ΔF/sec) for near membrane ΔpH_c triggered by L- (n = 5) or D-lactate (n = 5) in Ringer's solution of pH 7.4

*p < 0.05, **p < 0.01, by paired *t*-test.

membrane extracellular protons, we monitored the near membrane changes of pH_c by expressing ASIC1a that contained a yellow fluorescent protein (YFP) tag at its C-terminus (ASIC1a-YFP). YFP fluorescence is known to be quenched easily by protons and thus the fluorescence of ASIC1a-YFP expressing cells is strongly influenced by the local pH change near the plasma membrane at the cytoplasmic side. We found that similar to the results obtained with ASIC1a-pHluorin, L-lactate also induced a faster and greater decrease of the YFP fluorescence in the ASIC1a-YFP expressing cells than D-lactate (Fig. 4F–H). That the pH changes at the extracellular side near ASIC1a closely match the local pH decreases at the cytoplasmic side of the channel upon exposure of the cell to L- and D-lactate indicates that the extracellular acidification most likely resulted from the proton extrusion by the cell following the lactate uptake and subsequent pH_c drop.

Calcium is a critical accelerator of the mitochondrial metabolic rate in neurons. We thus asked if the activation of ASIC1a by L-lactate, which triggers $[Ca^{2+}]_c$ and $[Ca^{2+}]_m$ responses, could lead to enhanced mitochondrial metabolic activity. To address this question, we compared mitochondrial metabolic rates between cortical neurons prepared from WT and *Asic1a* KO mice by seahorse analysis (Fig. 5) where we pretreated the neurons with lactate thus simulating the long lasting production of lactate by astrocytes [16]. We found that in WT neurons, maximal respiration rates were higher if the medium contained 5 mM L-lactate, than if it contained 5 mM D-lactate, or no lactate at all (Fig. 5A, B). However, the presence of L-lactate did not affect respiration of *Asic1a* KO neurons (Fig. 5C, D), indicating that the lactate-induced Ca^{2+} signaling mediated by ASIC1a is communicated to the mitochondria leading to enhanced metabolic rate. We also determined that the maximal respiration rate of WT neurons was higher than that of *Asic1a* KO neurons in the presence of L-lactate (Fig. 5E, F). Furthermore, following the lead that lactate transporters are essential for the L-lactate evoked, ASIC1a-dependent, Ca^{2+} responses in the cytosol and mitochondria (Fig. 3), CIN4 abolished the effect of L-lactate on accelerating respiration rates in WT neurons (Fig. 5G, H, more complete summary data in Supplementary Fig. 3A, B). For comparison, we also measured ECAR rates under the same conditions as that used for oxidative phosphorylation by performing ECAR analysis (Supplementary Fig. 3C-E). In the presence of L-lactate, the basal ECAR rate was decreased in the WT, but not *Asic1a* KO, neurons and the decrease was inhibited by the treatment with CIN4. Thus, the increased respiration caused by L-lactate

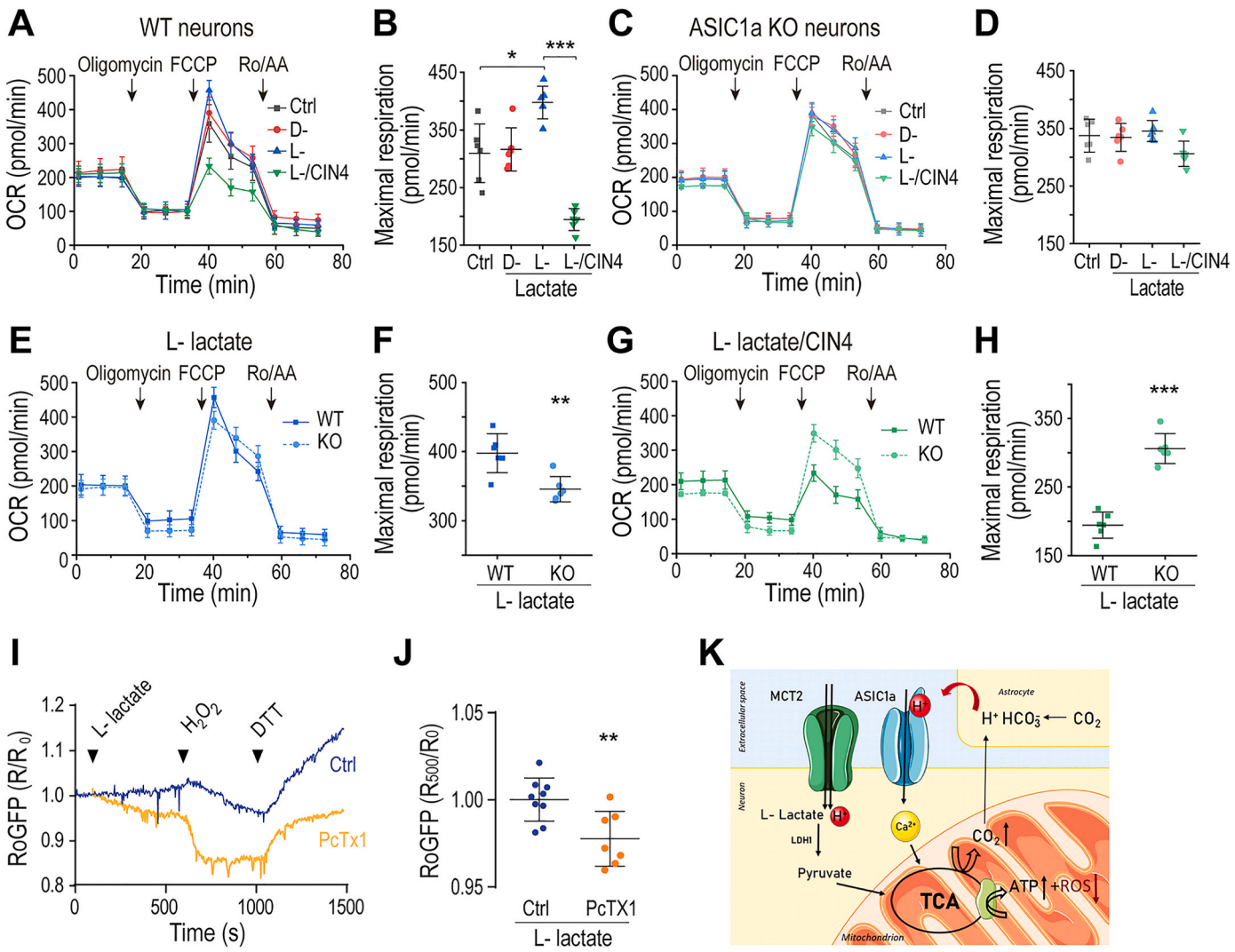

Fig. 5. ASIC1a mediates L-lactate-induced increase in mitochondrial respiration and suppresses mitochondrial ROS production.
Seahorse analysis (see Materials and Methods) was used to monitor mitochondrial respiration (OCR) with sequential additions of oligomycin (1 μM), FCCP (1 μM) + sodium pyruvate (5 mM), and a mix of rotenone/antimycin A (Ro/AA, 0.5 μM each), as indicated by the arrowheads, in media that contained or not D-, or L-lactate (5 mM);
(A) Representative OCR plots of WT neurons in regular medium that contained no lactate (Ctrl) or the indicated lactate isomer and CIN4;
(B) Quantification of maximal respiration as measured in (A) of WT neurons in regular medium (n = 6), and the medium that contained D- (n = 6) or L-lactate (n = 6), or L-lactate plus CIN4 (n = 6);
(C) Representative OCR plots of KO neurons in regular medium or medium that contained the indicated lactate isomer and CIN4;
(D) Quantification of maximal respiration as measured in (C) of KO in regular medium (Ctrl, n = 6) and media that contained the indicated D-lactate (n = 6), L-lactate (n-6), and L-lactate + CIN4 (n = 6);
(E) Representative OCR plots of WT and KO neurons in L -lactate containing medium;
(F) Quantification of maximal respiration as measured in (E) of WT (n = 6) and KO (n = 6) neurons;
(G) Representative OCR plots of WT and KO neurons in L-lactate/CIN4 containing medium (n = 6);
(H) Quantification of maximal respiration as measured in (G) of WT and KO neurons in L -lactate/CIN4 containing medium (n = 6 for each);
(I) Representative RoGFP fluorescence traces for redox changes in response to L-lactate, H_2O_2 and DTT added in the Ringer's solution in WT neurons untreated and treated with PcTX1;
(J) Quantification of R/R_0 (480/405) at 500s after the addition of L-lactate (100s) as in (I) for WT neurons untreated (n = 9) and treated with PcTX1 (n = 7);
(K) Schematic presentation of suggested pathway linking L-lactate to ASIC1a.
All summary graph data represent mean ± SD, *p < 0.05, **p < 0.01, ***p < 0.001.

was accompanied with a decrease in ECAR in WT neurons, which did not occur in the absence of ASIC1a or when lactate transport was blocked.

Mitochondrial redox state is controlled by $[Ca^{2+}]_m$ transients. We therefore asked if L-lactate affects the mitochondrial redox response and if ASIC1a is engaged in such response. To monitor the mitochondrial redox state, we expressed the redox sensor RoGFP that targets the mitochondrial matrix in neurons. While in the absence of PcTX1, the application of L-lactate triggered minimal fluorescence ratio changes of RoGFP, in the presence of PcTX1, it induced a marked decrease of RoGFP ratio, indicative of oxidation in mitochondria (Fig. 5I, J). These results indicate a critical role of ASIC1a in suppressing mitochondrial ROS production caused by L-lactate. Intriguingly, ASIC1a also slowed down mitochondrial ROS increase elicited by H_2O_2, as shown by the faster decrease of the RoGFP ratio in the presence of PcTX1 (Fig. 5 I), suggesting that ASIC1a plays a general and important role in regulating redox balance in mitochondria.

3. Discussion

ASIC1a is commonly studied in the context of large extracellular pH changes such as during synaptic transmission or in pathophysiological acidosis [23,24]. We recently showed that ASIC1a-dependent cytosolic and mitochondrial Na^+ and Ca^{2+} fluxes are also evoked by physiological pH changes (to pH 7.0), thereby modulating mitochondrial metabolic activity and respiration of neurons [8]. Here we focused on physiological L-lactate as a key metabolite required for neuronal activity. Previous studies have indicated that lactate exerts a potentiation effect on ASIC1a through its weak divalent cation binding capability that removes the inhibitory Ca^{2+}/Mg^{2+} from the ASIC1a channel pore [13]. Our results suggest that in addition to this effect, the physiologically relevant L-isomer of lactate at the physiological concentration of 2–5 mM also induces ASIC1a activation through an indirect mechanism that lowers the extracellular pH in the vicinity of the ASIC1a channel and through this pathway L-lactate stereo-selectively enhances the mitochondrial metabolic rate in neurons.

Our findings differ from the previous results in several important aspects. First, the concentration of lactate required to trigger an ASIC1a-dependent $[Ca^{2+}]_c$ and $[Ca^{2+}]_m$ response is 2–5 mM, much lower than the concentration (15 mM) required to chelate divalent cations (Ca^{2+} and Mg^{2+}) so as to keep them out of the ASIC1a pore [13]. Second, we show a stereo-selectivity for the L-, but not D-, isomer of lactate to elicit the ASIC1a-dependent $[Ca^{2+}]_c$ and $[Ca^{2+}]_m$ signals. This contrasts the chelating effect of lactate, which implied that the L- and D-isomers of lactate should have a similar efficacy in chelating the divalent cations and potentiating ASIC1a channel function. Third, we show that the stereo-selectivity of L-lactate on ASIC1a activation arises from the lactate transporter-mediated uptake, which in turn causes cytosolic acidification due to protons dissociated from lactate in the cytosolic environment and/or its metabolism [25]. We demonstrate that although both L- and D-lactate can penetrate the cell membrane and cause time-dependent pH_c decreases, the rate of pH_c decrease, reflective of lactate uptake, was much faster for L-lactate than D-lactate. Such a difference in the acidification rate also occurred in the vicinity of ASIC1a at both inside and outside of the plasma membrane. While our results argue against a Mg^{2+} chelating effect under physiological Mg^{2+} concentration, a recent study unveiled a novel and intriguing signaling role of lactate in regulating metabolic activity through Mg^{2+} [26]. It was shown that L-lactate at physiological concentration triggers release from the endoplasmic reticulum of Mg^{2+}, which is then taken via the MRS2 channel into the mitochondria. The rise in mitochondrial Mg^{2+} seems to mitigate the mitochondrial metabolic rate. Thus, lactate appears to be a pleiotropic signaling factor in shaping metabolic activity. It will be of interest to determine in future studies how these distinct lactate signaling pathways interact.

Lactate is a weak acid that can permeate the cell membrane in its protonated form; this may account for the slow uptake of D-lactate and the residual uptake of L-lactate in the presence of the lactate transporter inhibitor, CIN4. The importance of lactate transporters in mediating the stereo-selective effect of L-lactate at its physiological concentrations on ASIC1a in neurons is thus demonstrated by the greatly attenuated $[Ca^{2+}]_c$ and $[Ca^{2+}]_m$ signals in neurons stimulated either with D-lactate or with L-lactate but having the lactate transporters blocked by CIN4 or the shRNA-mediated knockdown of MCT2. This mechanism of action is completely distinct from the divalent chelating effect of the weak acid. Finally, whereas the effect of L-lactate on ASIC1a activation was detected by presenting the compound in the pH 7.4 Ringer's solution, the divalent chelating-based potentiation effect required a minimum of extracellular acidification of pH 7.0 in order to emerge [13].

ASIC1a is activated by protons from the extracellular side. Using extracellular pHluorin-tagged ASIC1a and GluR2, we detected near membrane extracellular acidification in response to lactate, with the L-isomer inducing faster and more robust pH decrease than the D-isomer. These differences in the rates and maximal magnitudes of pH decreases between L-lactate and D-lactate resembled that in the cytosol, as assessed for both the global pH_c changes using BCECF and local near membrane pH changes using YFP attached to the cytoplasmic C-terminus of ASIC1a.

Although as a weak acid, lactate could theoretically stimulate ASIC1a by directly lowering extracellular pH, our results provide at least two arguments against such a scenario. First, lactate activated ASIC1a-dependent Ca^{2+} signaling when applied at a neutral pH of 7.4. Second, the stereo-selectivity is not expected if lactate activates ASIC1a by directly acidifying the extracellular environment. The inhibitory effect of CIN4 and MCT2 shRNA suggests that lactate permeation into the neuron is necessary to evoke the ASIC1a-dependent Ca^{2+} signaling. Collectively, these data clearly demonstrate a pathway that involves stereo-selective uptake of L-lactate by lactate transporters, intracellular acidification and the subsequent proton extrusion from the cell to activate the plasma membrane bound ASIC1a channels by protons from the extracellular side. The activated ASIC1a then mediates Ca^{2+} influx, which generates $[Ca^{2+}]_c$ signals that propagate into the mitochondria.

The extracellular acidification caused by the above mechanism is expected to be weak. Previously, we showed that even with the mild extracellular pH drop from 7.4 to 7.0, which occurs within the normal physiological range, ASIC1a is activated to generate sufficient $[Ca^{2+}]_c$ signal that is transmitted to mitochondria to enhance mitochondrial respiration [8]. Similarly, here we show that the application of the physiological concentration of L-lactate not only triggers $[Ca^{2+}]_c$ and $[Ca^{2+}]_m$ signals via ASIC1a, but is also sufficient to accelerate ASIC1a-dependent mitochondrial respiration. Thus, the moderate extracellular acidification resulting from stereo-selective uptake of L-lactate at the neutral pH exerts similar actions on Ca^{2+} signaling and mitochondrial metabolism as the mild extracellular pH drop. $[Ca^{2+}]_m$ rise is a major up-regulator of metabolic activity [27]. Our results identify ASIC1a as a metabolic sensor that is tuned up by neuronal acid extrusion triggered by L-lactate uptake through lactate transporters. The resulting Ca^{2+} signal transmitted by the ASIC1a channel is propagated from the cytosol to the mitochondria, accelerating the mitochondrial catabolic processing of the lactate (Fig. 5K). It remains unclear what is the acid extrusion pathway that is triggered by the lactate dependent pH_c drop. Na^+/H^+ exchanger 1 (NHE1) is allosterically activated by pH_c drop and is a major acid extruder in neurons [28]. Interestingly, the KO of NHE1 similarly to KO of ASIC1a leads to brain damage although the effect of NHE1 is stronger, indicating its pleotropic roles [28]. Further studies are, however, required to firmly establish if NHE1 is involved in the L-lactate-evoked ASIC1a activation.

Importantly, the ASIC1a-dependent metabolic boost appears to protect mitochondria from oxidative stress induced by lactate, and even the subsequently added H_2O_2. The association between $[Ca^{2+}]_m$ and ROS production is complex. Recent studies indicate that it is biphasic and linked to the energetic status of the cell [29]. Calcium is a major regulator of the mitochondrial electron transport chain and the Krebs cycle. On the other hand, $[Ca^{2+}]_m$ overload has a well-documented detrimental role on these pathways [30]. Thus, in the presence of metabolic substrate and low Ca^{2+}, the imbalance between their metabolic oxidation and the electron transport rate may trigger ROS production. Also, Ca^{2+} overload, a hallmark of major brain syndromes, will impair electron transport chain similarly leading to enhanced ROS production [31]. Our Ca^{2+} imaging and metabolic results indicate that ASIC1a acts by delivering the optimal $[Ca^{2+}]_m$ dose that facilitates an efficient metabolic consumption of lactate while minimizing ROS production. Moreover, given that $[Ca^{2+}]_c$ increase can trigger non mitochondrial ROS production [32], further studies are required to determine to what extent the $[Ca^{2+}]_c$ rise triggered by lactate contributes to mitochondrial redox balance through non-mitochondrial ROS production. Furthermore, our data may also explain the double-edged sword role of ASIC1a. This channel is important for proper brain function [33,34] whereas it also contributes to ischemic brain damage [35]. Our results suggest that by mediating Ca^{2+} signaling ASIC1a tunes the

metabolic activity to optimum when oxygen and metabolites are present (Fig. 5K). Further studies are required to identify the detailed metabolic implication of ASIC1a lactate axis on respiratory and the glycolytic pathway. During ischemic insult oxygen deprivation curtails the metabolic effect of ASIC1a, but the ASIC1a dependent $[Ca^{2+}]_m$ rise adds to the burden of mitochondrial Ca^{2+} overload. This is expected to trigger a dual ROS production and mitochondrial depolarization culminating in a "2 hit scenario" [36] required for robust mitochondrial permeability transition pore opening, which often leads to neuronal death.

4. Materials and methods

4.1. Primary neuronal culture

We used wild-type - WT (Envigo, C57BL cat #6JRCCH5B043) [37] and ASIC1a KO mice (kind gifts of Prof. Michael J. Welsh (Howard Hughes Medical Institute, University of Iowa, Iowa City, IA, USA)) both derived from C57BL/6J background. Animals were generated and maintained as previously described [23] with the approvals and in accordance with the guidelines of the Ben-Gurion University Institutional Committee for Ethical Care and Use of Animals in Research (Reference Number: IL 07-02-2019C) and of the Animal Ethics Committee of Shanghai Jiao Tong University School of Medicine (Reference number: DLAS-MP-ANIM.01-05).

Hippocampal and cortical neuronal cultures were prepared as previously described [8]. Briefly, mice were housed in specific pathogen free facilities. Rodent care practices were under sterile conditions, with sterile supplies. Rodent housing conditions were: 12:12 light: dark cycles at 20–24 °C and 30–70% relative humidity. Animals were free fed autoclaved rodent chow and had free access to reverse osmosis filtered water. Rodents were housed in individually ventilated GM500 (Tecniplast, Italy) cages in groups of maximum 5 mice per cage.

Primary culture of hippocampal neurons was prepared for each independent experiment from mouse pups. Glass coverslips (13-mm, Thermo Scientific, cat # BNCB00130RA1N) placed individually into wells of a 24-well plate or glass bottom dishes (Glass Bottom Dish/29 mm Dish with 14-mm Bottom Well #0 Glass, Vendor: Cellvis Cat #D29-14-0-N) were coated with poly-D-lysine (Thermo Fisher Scientific, Cat #A3890401) overnight. Planting glass surfaces were washed with sterile double distilled water and stored protected from light for less than 24 h prior to cell seeding. Each mouse pup hippocampus was used to generate 6 coverslips with 50,000 to 70,000 cells.

The hippocampi were carefully dissected and separated from the rest of the brain. The dissected tissues were treated with digestion solution [4 ml HBSS (Biological Industry, Cat # 02-015-1 B) containing 1 ml of 20 mM HEPES (BioLab, Cat # 000804239100), pH 7.4, 75 μl 100 mM $CaCl_2$ (Sigma-Aldrich, Cat #C4901), 50 μl 50 mM EDTA (Sigma-Aldrich, Cat #E5134 pH 7.4), 0.0053 mg/μl cysteine crystals (Sigma Aldrich Cat #C7352) and 1 mg/ml papain (Worthington, Lakewood, Cat #LS003126)] at room temperature for 20 min and serially triturated. The dissociated neurons were plated onto the coated glass coverslips at the density of 50,000–70,000 neurons per well. Neurons were plated in plating medium consisting of Neurobasal-A medium (Thermo Fisher Scientific, Cat #21103049) supplemented with 5% defined fetal bovine serum (FBS, Hyclone Life Science, Cat #SH30070.03), 2% B27 (Thermo Fisher Scientific, Cat #17504044), 2 mM Glutamax I (Life Technologies, Cat #35050038), and 1 μg/ml gentamicin (Thermo Fisher Scientific, Cat #15750060). After 24 h, the plating medium was replaced by a serum-free culture medium consisting of Neurobasal-A, 2% B27, and 2 mM Glutamax I. Cultures were typically maintained at 37 °C in a 5% CO_2 humidified incubator for 10–15 days before experimentation. Neurons were easily distinguishable from glia: they appeared phase bright, had smooth rounded somata and distinct processes, and laid just above the focal plane of the glial layer.

ASIC1a KO related experiments were done using cortical neurons cultured on glass bottom dishes as described previously [8]. The cortex was carefully dissected and separated from the rest of the brain. The dissected tissues were incubated with 0.05% trypsin-EDTA for 15 min at 37 °C, followed by trituration with pipette tips. The dissociated neurons were plated onto the coated glass coverslips and cultured in Neurobasal medium supplemented with 2% B27 and 2 mM Glutamax. Cultures were typically maintained at 37 °C in a 5% CO_2 humidified incubator for 10–15 days before experimentation. Cultures were fed twice a week.

4.2. Cell line and transfection

CHO cells (ATCC, CCL-61) were cultured on #0 cover glass with F12 medium supplemented with 2 mM L-glutamine and 10% FBS (Gibco), and transiently transfected with cDNA constructs using Hilymax (Dojindo laboratories, Cat #H357) following the manufacturer's protocol. Cells were used within 1–2 days after transfection.

4.3. Generation of pAAV2 mtRoGFP biosensor and virus preparation

RoGFP matrix sensor that expresses thiol redox-sensitive ratiometric sensor RoGFP in the mitochondrial matrix of mammalian cells was purchased from Addgene [38] (Cat #49437). Viral particles were prepared as described previously [39]. Briefly, cDNA of interest (mtRoGFP from RoGFP matrix) was subcloned by restriction/ligation into a plasmid containing adeno-associated virus 2 (AAV2) inverted terminal repeats flanking a cassette consisting of the 0.47 kb human synapsin 1 promoter (hSyn) [40], the woodchuck post-transcriptional regulatory element and the bovine growth hormone polyA signal. Viral particles were produced in HEK-293 cells using both the pD1 and pD2 helper plasmids [41], which encode the rep/cap proteins of AAV1 and AAV2, respectively. Primary cultures of hippocampal neurons were infected at days in vitro (DIV) 5 and the culture continued for at least 7 days before imaging. Virion titer was individually adjusted to produce 75–90% infection efficiency.

4.4. Fluorescence imaging

Experiments done on WT neurons, untreated or treated with PcTX1 (Alomone labs, #STP200), were performed using the imaging system consisted of an Axiovert 100 inverted microscope (Zeiss), Polychrome V monochromator (TILL Photonics, Planegg, Germany) and a SensiCam cooled charge-coupled device (PCO, Kelheim, Germany). Cells seeded on the glass coverslips, as described previously, were positioned to a special holder designed to enable constant flow of solutions without changing the definite amount of perfusion solution and thus the imaging focus. Fluorescent images were acquired with Imaging WorkBench 4.0 (Axon Instruments, Foster City, CA) using magnification of 10x for cytosolic and 20x for mitochondrial measurements. Acquisition speeds were 1 frame every 3 s for mitochondrial Ca^{2+} measurements, 1 frame every 1.5 s for cytolsolic Ca^{2+} measurements, and 1 frame every 3 s for cytosolic pH measurements.

The dish was mounted on the stage of an inverted fluorescence microscope (Nikon Eclipse TI, Japan) and neurons were observed with a 20× objective lens. The fluorescence images were acquired while neurons were continuously perfused. Puff perfusion changes were achieved with the use of the ALA-VM8 8 valve manifold for perfusion system whose tip was placed approximately 500 μm from neurons and the velocity of the flow was ~350 μl/min.

In all fluorescent experiments, cells were pre-loaded with the indicated ion specific fluorescent dye at the indicated concentrations for 30 min at room temperature using Ringer's solution containing (in mM): 126 NaCl, 5.4 KCl (Sigma-Aldrich, Cat #P9333), 0.8 $MgCl_2$, 20 HEPES, 1.8 $CaCl_2$, 15 glucose (Gerbu, Cat #2028), with pH adjusted to 7.4 with NaOH (Sigma-Aldrich, Cat #221465) and supplemented with 0.1% bovine serum albumin (BSA, VWR, Cat #0332). After loading, cells were washed quickly 3 times and then incubated for 30 min in the dye-free Ringer's solution.

At the beginning of each experiment, cells were perfused with Ca^{2+}-containing Ringer's solution supplemented with 0.1% BSA. To trigger ionic responses, cells were perfused with the Ringer's solution of the same compositions and pH adjusted to 7.4 by NaOH (Sigma-Aldrich, Cat #221465) after DL-, D- or L-lactate addition.

$[Ca^{2+}]_c$ was monitored in cells loaded with Ca^{2+} specific ratiometric dye Fura-2 AM (Sigma Aldrich, Cat #F0888) (1 μM), which were illuminated alternately with 340 nm and 380 nm excitations and imaged with a 510 nm long pass filter. Fluo-4 AM (Dojindo, Cat #F312) (2 μM) was also used for $[Ca^{2+}]_c$ detection in some experiments with 488 nm wavelength light for excitation. $[Ca^{2+}]_m$ was measured in cells loaded with Ca^{2+} specific dye Rhod-2 AM (Biotium, Cat #50024) (1 μM) that preferentially localizes in mitochondria. Rhod-2 was excited at 552 nm wavelength light and imaged with a 570 nm-long pass filter as previously described [42].

Cytosolic pH changes were measured in cells preloaded with BCECF AM [2′, 7′-bis-(2-carboxyethyl)-5-(and-6-) carboxyfluorescein AM] (25 μM, TefLabs) for 15 min in the presence of 0.02% pluronic acid as described previously [43]. Images were obtained with a band-pass emission filter of 535 nm, while R represents the ratio of the emitted signal obtained using excitation wavelengths of 440 nm/480 nm.

PcTX1 treatment was performed prior to each fluorescent imaging experiment for 120s in a concentration of 20 nM, known to block ASIC1a [44,45].

pHluorin experiments were done using CHO cells cultured on glass bottom dishes and transfected with pHluorin plasmid. The dish was mounted on the stage of an inverted fluorescence microscope (Nikon Eclipse TI, Japan) and CHO cells were observed with a 20× objective lens. The fluorescence images were acquired while cells were continuously perfused. Puff perfusion changes were achieved with the use of the ALA-VM8 8 valve manifold for perfusion system whose tip was placed approximately 500 μm from CHO and the velocity of flow was ~350 μl/min. The perfusate was switched from Ca^{2+}-containing Ringer's solution supplemented with 0.1% BSA to Ringer's solution of the same compositions and pH adjusted to 7.4 by NaOH after DL-, D- or L-lactate addition. Extracellular acidification was monitored by the fluorescence of pHluorin with 488 nm excitation and imaging with a band-pass emission filter of 535 nm.

YFP experiments were done using CHO cells cultured on glass bottom dishes and transfected with ASIC1a-YFP plasmid. Cytoplasmic near plasma membrane acidification was monitored by the fluorescence of YFP with 488 nm excitation and imaging with a band-pass emission filter of 535 nm.

Ratiometric measurements of the mitochondrial redox state were performed using the same instrument as described above for hippocampal neurons infected with AAV2 viral vector containing the mitochondrial targeted, genetically encoded sensor RoGFP [38]. Cells were imaged at excitations of 405 and 480 nm and emission at 535 nm every 3 s. The 405/480 fluorescence ratios were normalized by obtaining the minimum and maximum ratios after addition of 1 mM H_2O_2 and of 10 mM DTT, respectively [46]. The fluorescence signals of RoGFP (R) were normalized to the averaged baseline signal (R_0) obtained at the beginning of the measurements.

4.5. Oxygen consumption measurements

Primary cultured cortical neurons were typically maintained at 37 °C in a 5% CO_2 humidified incubator for 10–15 days before experimentation. At 24 h before the experiment, neurons were seeded on poly-D-lysine-coated 96-well seahorse plates (Agilent, Cat #103730-100) and grown in the planting medium. Cartridge was immerged in XF calibrant solution (Agilent, Cat #100840-000) and placed in a CO_2 free incubator until use. Seahorse working protocol was carried out as described before [47]. Briefly, on the day of the experiment, 2 h before oxygen consumption measurements, medium was replaced by Seahorse XF DMEM (Cat # 103575-100), consisting of 143 mM NaCl, 5.4 mM KCl, 0.91 mM NaH_2PO_4, 0.8 mM $MgCl_2$, 1.8 mM $CaCl_2$, and 15 mg/ml phenol red, with no glucose, glutamine or pyruvate, and with D- or L-lactate (5 mM) added as needed. Neurons were kept at 37 °C without CO_2 to evoke glycolysis. During these 2 h, ports of cartridge containing the oxygen probes were loaded with the compounds to be injected during the assay and the cartridge was calibrated. OCR was measured in non-treated or 5 mM lactate and/or 250 nM CIN4 -treated neurons. Basal respiration was recorded 3 times for 18 min until system stabilization. FCCP was used at a final concentration of 1 μM and injected with sodium pyruvate (Sigma Aldrich, Cat #P2256) at a final concentration of 5 mM. Oligomycin (Sigma-Aldrich, Cat #75351) and a mix of rotenone/antimycin A (Aligent, Cat #103015-100) were used at final concentrations of 1 μM and 0.5 μM, respectively. For non-mitochondrial metabolic analysis, extracellular acidification rate (ECAR) was measured. All respiratory modulators were used at optimal concentrations titrated during preliminary optimization experiments (data not shown). The assay was performed using Seahorse Bioscience XF96 extracellular flux analyzer and the data were exported from the Wave (Seahorse official) software.

4.6. Construction of MCT2 shRNA with lentiviral vector and virus preparation

For MCT2 knockdown, three targeting shRNA vectors were constructed into pMagic 7.1 lentiviral plasmid using *Age*I and *Eco*RI cloning sites. The following pairs of oligonucleotides were used to target MCT2: 1#: 5′-CCGGGCTGCATTGGAATGATCTTGGCTCGAGCCAAGATCATTCCAATGCAGCTTTTTTG-3; 2#: 5'-CCGGTTCATTGGAGGTTTAGGATTACTCGAGTAATCCTAAACCTCCAATGAATTTTTTG-3; 3#: 5'-CCGGGCTTAATCCGTCCACGAATCCCTCGAGGGATTCGTGGACGGATTAAGCTTTTTTG-3. Lentivirus was prepared as previously described [48]. Primary cortical neurons were infected at DIV 10 and then cultured for 48 h before experimentation.

4.7. Western blot analysis

Cells were harvested by 1 × RIPA buffer (Beyotime, Cat #P0013B) containing 2 mM PMSF (Cell Signaling Technology, Cat #8553), 1 × Protease inhibitor cocktail (Beyotime, Cat #P1006) and 1 × Phosphatase Inhibitor Cocktail (Cell Signaling Technology, Cat #5870). Protein content was quantified by Pierce BCA Protein Assay (Thermo Scientific, Cat #23225). Lysates were separated on SDS-PAGE and transferred to Immobilon®-P Transfer Membrane (Millipore, Cat #C3117). After blocking in 5% skim milk for 1 h, membranes were incubated at 4 °C overnight with primary antibodies: anti-MCT2 antibody (Santa Cruz, Cat #sc-166925) and β-actin (Millipore, Cat #MAB1501, all diluted at 1:1000). After washing, membranes were incubated in relevant secondary HRP-conjugated antibodies. The signal was detected after incubation with SuperSignal West Pico PLUS Chemiluminescent Substrate (Thermo Scientific, Cat #34580) by ImageQuant LAS4000 Molecular Imaging System (GE Healthcare Life Sciences) and quantified using the ImageJ gray analysis method.

4.8. Statistical analysis

For each figure at least 3 experiments from independent cell cultures were conducted. In each of them traces were obtained from at least 3 samples of 3 regions of interest of at least 5 cells, in a non-blind manner and plotted using KaleidaGraph. All independent data points were included in the statistical analysis using 2 tailed unpaired Student's *t*-test after individual data point were analyzed for normality using Kolmogorov–Smirnov test. Only data that passed this latter analysis were included in the analysis for significance. For multiple condition treatment, one-way ANOVA was applied for statistical analysis and Tukey test for means comparison. No randomization or sample size calculation was performed, and the study was not preregistered. The study was exploratory, no exclusion of data was required, and no specific test for

outliers was predetermined or required. GraphPad Prism 6 software was used for statistical analysis and Adobe Illustrator for the graphic design of the figures. All summary data are presented as average of at least 3 (n) independent measurements ± SD, each containing multiple repetitions of 10–99 single cells in imaging studies or wells in metabolic analysis. A value of $p < 0.05$ was accepted as statistically significant. Symbols of significance used: *$p < 0.05$, **$p < 0.01$, ***$p < 0.001$, ****$p < 0.0001$.

Declaration of competing interest

Authors declare no conflict of interest.
All authors declare that there are no conflicting interests.

Acknowledgments

This study was supported by grants from the National Natural Science Foundation of China (81730095) to T.L.X, the Innovative Research Team of High-level Local Universities in Shanghai, Science and Technology Commission of Shanghai Municipality (18JC1420302) to T.L.X, the Shanghai Municipal Science and Technology Major Project (2018SHZDZX05) to T.L.X, NIH (NS102452) to M.X.Z. and ISF China (1210/14) to T.L.X. and I.S.

Appendix A. Supplementary data

Supplementary data to this article can be found online at https://doi.org/10.1016/j.redox.2022.102253.

References

[1] O. Krishtal, The ASICs: signaling molecules? Modulators? Trends Neurosci. 26 (2003) 477–483.
[2] L.J. Wu, B. Duan, Y.D. Mei, J. Gao, J.G. Chen, M. Zhuo, L. Xu, M. Wu, T.L. Xu, Characterization of acid-sensing ion channels in dorsal horn neurons of rat spinal cord, J. Biol. Chem. 279 (2004) 43716–43724.
[3] S.C. Grifoni, N.L. Jernigan, G. Hamilton, H.A. Drummond, ASIC proteins regulate smooth muscle cell migration, Microvasc. Res. 75 (2008) 202–210.
[4] H. Jahr, M. van Driel, G.J. van Osch, H. Weinans, J.P. van Leeuwen, Identification of acid-sensing ion channels in bone, Biochem. Biophys. Res. Commun. 337 (2005) 349–354.
[5] R. Waldmann, G. Champigny, F. Bassilana, C. Heurteaux, M. Lazdunski, A proton-gated cation channel involved in acid-sensing, Nature 386 (1997) 173–177.
[6] S. Grunder, X. Chen, Structure, function, and pharmacology of acid-sensing ion channels (ASICs): focus on ASIC1a, Int. J. Physiol. Pathophysiol. Pharmacol. 2 (2010) 73–94.
[7] S. Grunder, M. Pusch, Biophysical properties of acid-sensing ion channels (ASICs), Neuropharmacology 94 (2015) 9–18.
[8] I. Savic Azoulay, F. Liu, Q. Hu, M. Rozenfeld, T. Ben Kasus Nissim, M.X. Zhu, I. Sekler, T.L. Xu, ASIC1a channels regulate mitochondrial ion signaling and energy homeostasis in neurons, J. Neurochem. 153 (2020) 203–215.
[9] A. Baron, L. Schaefer, E. Lingueglia, G. Champigny, M. Lazdunski, Zn^{2+} and H^+ are coactivators of acid-sensing ion channels, J. Biol. Chem. 276 (2001) 35361–35367.
[10] X.P. Chu, J.A. Wemmie, W.Z. Wang, X.M. Zhu, J.A. Saugstad, M.P. Price, R. P. Simon, Z.G. Xiong, Subunit-dependent high-affinity zinc inhibition of acid-sensing ion channels, J. Neurosci. : Off. J Soc. Neurosci. 24 (2004) 8678–8689.
[11] C. Gonzalez-Inchauspe, M.N. Gobetto, O.D. Uchitel, Modulation of acid sensing ion channel dependent protonergic neurotransmission at the mouse calyx of Held, Neuroscience 439 (2020) 195–210.
[12] D. Wang, L. Li, J. Fuhrman, S. Ferguson, H. Wang, The role of constitutive androstane receptor in oxazaphosphorine-mediated induction of drug-metabolizing enzymes in human hepatocytes, Pharmaceut. Res. 28 (2011) 2034–2044.
[13] D.C. Immke, E.W. McCleskey, Lactate enhances the acid-sensing Na^+ channel on ischemia-sensing neurons, Nat. Neurosci. 4 (2001) 869–870.
[14] H. Wang, D.W. Wu, X.M. Chen, C. Li, S.F. Ding, Q. Zhai, B.F. Du, Y. Li, K.F. Wang, [Relationship between blood lactic level, lactic clearance, duration of lacticemia and prognosis of critically ill patients in intensive care unit], Zhongguo wei zhong bing ji jiu yi xue = Chinese critical care medicine = Zhongguo weizhongbing jijiuyixue 21 (2009) 357–360.
[15] T. Ohbuchi, K. Sato, H. Suzuki, Y. Okada, G. Dayanithi, D. Murphy, Y. Ueta, Acid-sensing ion channels in rat hypothalamic vasopressin neurons of the supraoptic nucleus, J. Physiol. 588 (2010) 2147–2162.
[16] L. Pellerin, G. Pellegri, P.G. Bittar, Y. Charnay, C. Bouras, J.L. Martin, N. Stella, P. J. Magistretti, Evidence supporting the existence of an activity-dependent astrocyte-neuron lactate shuttle, Dev. Neurosci. 20 (1998) 291–299.
[17] J.G. McCormack, R.M. Denton, Intracellular calcium ions and intramitochondrial Ca^{2+} in the regulation of energy metabolism in mammalian tissues, Proc. Nutr. Soc. 49 (1990) 57–75.
[18] E.J. Griffiths, G.A. Rutter, Mitochondrial calcium as a key regulator of mitochondrial ATP production in mammalian cells, Biochim. Biophys. Acta 1787 (2009) 1324–1333.
[19] M. Nedergaard, S.A. Goldman, Carrier-mediated transport of lactic acid in cultured neurons and astrocytes, Am. J. Physiol. 265 (1993) R282–R289.
[20] P.D. Bosshart, D. Kalbermatter, S. Bonetti, D. Fotiadis, Mechanistic basis of L-lactate transport in the SLC16 solute carrier family, Nat. Commun. 10 (2019) 2649.
[21] P.D. Bosshart, D. Kalbermatter, S. Bonetti, D. Fotiadis, Structure and function of a monocarboxylate transporter homolog specific for L-lactate, Molecul. Cell. Oncol. 6 (2019), e1646605.
[22] X.L. Song, D.S. Liu, M. Qiang, Q. Li, M.G. Liu, W.G. Li, X. Qi, N.J. Xu, G. Yang, M. X. Zhu, T.L. Xu, Postsynaptic targeting and mobility of membrane surface-localized hASIC1a, Neurosci. Bullet. 37 (2021) 145–165.
[23] J.A. Wemmie, J. Chen, C.C. Askwith, A.M. Hruska-Hageman, M.P. Price, B. C. Nolan, P.G. Yoder, E. Lamani, T. Hoshi, J.H. Freeman Jr., M.J. Welsh, The acid-activated ion channel ASIC contributes to synaptic plasticity, learning, and memory, Neuron 34 (2002) 463–477.
[24] L. Tian, J.H. Wang, M. Zhao, Y.C. Bao, J.F. Shang, Q. Yan, Z.C. Zhang, X.Z. Du, H. Jiang, R.J. Sun, B. Yuan, X.H. Zhang, T.Z. Zhang, X.L. Li, [Effect of scalp-acupuncture stimulation on neurological function and expression of ASIC 1 a and ASIC 2 b of hippocampal CA 1 region in cerebral ischemia rats], Zhen ci yan jiu = Acupuncture research 41 (2016) 417–422.
[25] A. de Hemptinne, R. Marrannes, B. Vanheel, Influence of organic acids on intracellular pH, Am. J. Physiol. 245 (1983) C178–C183.
[26] C.C. Daw, K. Ramachandran, B.T. Enslow, S. Maity, B. Bursic, M.J. Novello, C. S. Rubannelsonkumar, A.H. Mashal, J. Ravichandran, T.M. Bakewell, W. Wang, K. Li, T.R. Madaris, C.E. Shannon, L. Norton, S. Kandala, J. Caplan, S. Srikantan, P. B. Stathopulos, W.B. Reeves, M. Madesh, Lactate elicits ER-mitochondrial $Mg^{(2+)}$ dynamics to integrate cellular metabolism, Cell 183 (2020) 474–489 e417.
[27] Nicoletta Plotegher, Filadi Riccardo, Pizzo Paola, Duchen Michael R, Excitotoxicity Revisited: Mitochondria on the Verge of a Nervous Breakdown, Trends of Neuroscience 44 (5) (2021) 342–351, https://doi.org/10.1016/j.tins.2021.01.001.
[28] H. Yao, E. Ma, X.Q. Gu, G.G. Haddad, Intracellular pH regulation of CA1 neurons in Na(+)/H(+) isoform 1 mutant mice, J. Clin. Invest. 104 (1999) 637–645.
[29] J.F. Garbincius, J.W. Elrod, Mitochondrial calcium exchange in physiology and disease, In Press, Physiol. Rev. (2021).
[30] I. Drago, P. Pizzo, T. Pozzan, After half a century mitochondrial calcium in- and efflux machineries reveal themselves, EMBO J. 30 (2011) 4119–4125.
[31] Virani, S. S., Alonso, A., Aparicio, H. J., Benjamin, E. J., Bittencourt, M. S., Callaway, C. W., Carson, A. P., Chamberlain, A. M., Cheng, S., Delling, F. N., Elkind, M. S. V., Evenson, K. R., Ferguson, J. F., Gupta, D. K., Khan, S. S., Kissela, B. M., Knutson, K. L., Lee, C. D., Lewis, T. T., Liu, J., Loop, M. S., Lutsey, P. L., Ma, J., Mackey, J., Martin, S. S., Matchar, D. B., Mussolino, M. E., Navaneethan, S. D., Perak, A. M., Roth, G. A., Samad, Z., Satou, G. M., Schroeder, E. B., Shah, S. H., Shay, C. M., Stokes, A., VanWagner, L. B., Wang, N. Y., Tsao, C. W., American heart association council on, E., prevention statistics, C., and stroke statistics, S. (2021) heart disease and stroke statistics-2021 update: a report from the American heart association. Circulation 143, e254-e743.
[32] F.E. Oflaz, Z. Koshenov, M. Hirtl, R. Rost, O.A. Bachkoenig, B. Gottschalk, C. T. Madreiter-Sokolowski, R. Malli, W.F. Graier, Near-UV light induced ROS production initiates spatial Ca(2+) spiking to fire NFATc3 translocation, Int. J. Mol. Sci. 22 (2021).
[33] S.H. Lin, W.H. Sun, C.C. Chen, Genetic exploration of the role of acid-sensing ion channels, Neuropharmacology 94 (2015) 99–118.
[34] X.D. Ma, J.N. Song, M. Zhang, J.Y. An, Y.L. Zhao, B.F. Zhang, Advances in research of the neuroprotective mechanisms of cerebral ischemic postconditioning, Int. J. Neurosci. 125 (2015) 161–169.
[35] Z.G. Xiong, X.M. Zhu, X.P. Chu, M. Minami, J. Hey, W.L. Wei, J.F. MacDonald, J. A. Wemmie, M.P. Price, M.J. Welsh, R.P. Simon, Neuroprotection in ischemia: blocking calcium-permeable acid-sensing ion channels, Cell 118 (2004) 687–698.
[36] P.S. Brookes, Y. Yoon, J.L. Robotham, M.W. Anders, S.S. Sheu, Calcium, ATP, and ROS: a mitochondrial love-hate triangle, Am. J. Physiol. Cell Physiol. 287 (2004) C817–C833.
[37] D. Gitler, Y. Takagishi, J. Feng, Y. Ren, R.M. Rodriguiz, W.C. Wetsel, P. Greengard, G.J. Augustine, Different presynaptic roles of synapsins at excitatory and inhibitory synapses, J. Neurosci. : Off. J Soc. Neurosci. 24 (2004) 11368–11380.
[38] G.B. Waypa, J.D. Marks, R. Guzy, P.T. Mungai, J. Schriewer, D. Dokic, P. T. Schumacker, Hypoxia triggers subcellular compartmental redox signaling in vascular smooth muscle cells, Circ. Res. 106 (2010) 526–535.
[39] Y. Tevet, D. Gitler, Using FRAP or FRAPA to visualize the movement of fluorescently labeled proteins or cellular organelles in live cultured neurons transformed with adeno-associated viruses, Methods Mol. Biol. 1474 (2016) 125–151.
[40] S. Kugler, E. Kilic, M. Bahr, Human synapsin 1 gene promoter confers highly neuron-specific long-term transgene expression from an adenoviral vector in the adult rat brain depending on the transduced area, Gene Ther. 10 (2003) 337–347.
[41] A. Groh, C.P. de Kock, V.C. Wimmer, B. Sakmann, T. Kuner, Driver or coincidence detector: modal switch of a corticothalamic giant synapse controlled by spontaneous activity and short-term depression, J. Neurosci. : Off. J Soc. Neurosci. 28 (2008) 9652–9663.
[42] M. Kostic, M.H. Ludtmann, H. Bading, M. Hershfinkel, E. Steer, C.T. Chu, A. Y. Abramov, I. Sekler, PKA phosphorylation of NCLX reverses mitochondrial

calcium overload and depolarization, promoting survival of PINK1-deficient dopaminergic neurons, Cell Rep. 13 (2015) 376–386.
[43] D. Gilad, S. Shorer, M. Ketzef, A. Friedman, I. Sekler, E. Aizenman, M. Hershfinkel, Homeostatic regulation of KCC2 activity by the zinc receptor mZnR/GPR39 during seizures, Neurobiol. Dis. 81 (2015) 4–13, https://doi.org/10.1016/j.nbd.2014.12.020.
[44] M. Li, K. Inoue, D. Branigan, E. Kratzer, J.C. Hansen, J.W. Chen, R.P. Simon, Z. G. Xiong, Acid-sensing ion channels in acidosis-induced injury of human brain neurons, J. Cerebr. Blood Flow Metabol. : Off. J. Int. Soc. Cerebral Blood Flow Metabol. 30 (2010) 1247–1260.
[45] Y.Z. Wang, J.J. Wang, Y. Huang, F. Liu, W.Z. Zeng, Y. Li, Z.G. Xiong, M.X. Zhu, T. L. Xu, Tissue acidosis induces neuronal necroptosis via ASIC1a channel independent of its ionic conduction, Elife 4 (2015).
[46] T. Ben-Kasus Nissim, X. Zhang, A. Elazar, S. Roy, J.A. Stolwijk, Y. Zhou, R. K. Motiani, M. Gueguinou, N. Hempel, M. Hershfinkel, D.L. Gill, M. Trebak, I. Sekler, Mitochondria control store-operated Ca(2+) entry through Na(+) and redox signals, EMBO J. 36 (2017) 797–815.
[47] F.M. Cerqueira, B. Chausse, B.M. Baranovski, M. Liesa, E.C. Lewis, O.S. Shirihai, A. J. Kowaltowski, Diluted serum from calorie-restricted animals promotes mitochondrial beta-cell adaptations and protect against glucolipotoxicity, FEBS J. 283 (2016) 822–833.
[48] H. Wan, Q. Wang, X. Chen, Q. Zeng, Y. Shao, H. Fang, X. Liao, H.S. Li, M.G. Liu, T. L. Xu, M. Diao, D. Li, B. Meng, B. Tang, Z. Zhang, L. Liao, WDR45 contributes to neurodegeneration through regulation of ER homeostasis and neuronal death, Autophagy 16 (2020) 531–547.